Available online at www.sciencedirect.com
ScienceDirect
Proceedings of the Combustion Institute 31 (2007) 971–978
Proceedings of the Combustion Institute
www.elsevier.com/locate/proci

Computational and experimental study of a forced, time-dependent, methane–air coflow diffusion flame

S.B. Dworkin [a], B.C. Connelly [a], A.M. Schaffer [a], B.A.V. Bennett [a], M.B. Long [a], M.D. Smooke [a,*], M.P. Puccio [b], B. McAndrews [b], J.H. Miller [b]

[a] *Department of Mechanical Engineering, Yale University, New Haven, CT 06520-8284, USA*
[b] *Department of Chemistry, George Washington University, Washington, D.C. 20052, USA*

Abstract

Forced, time-varying flames are laminar systems that help bridge the gap between laminar and turbulent combustion. In this study, we investigate computationally and experimentally the structure of a periodically forced, axisymmetric laminar methane–air diffusion flame in which a cylindrical fuel jet is surrounded by a coflowing oxidizer jet. The flame is forced by imposing a sinusoidal modulation on the steady fuel flow rate. Rayleigh and spontaneous Raman scattering are used to generate the temperature and major species profiles. Particle image velocimetry is used to determine the magnitude of the velocity at the exit of the burner and the phase of the forcing modulation. CH^* flame emission measurements are used to provide an indication of the overall flame shape. Computationally, we solve the transient equations for the conservation of total mass, momentum, energy, and species mass with detailed transport and finite rate chemistry submodels. The governing equations are written using a modified vorticity–velocity formulation and are solved on an adaptively refined grid using implicit time stepping and Newton's method nested with a Bi-CGSTAB iterative linear system solver. Results of the study include an investigation of the start-up features of the time-dependent flames and the time it takes for initial transients to dissipate. We include a detailed description of the fluid dynamic-thermochemical structure of the flame at a 20 Hz forcing frequency for both 30% and 50% sinusoidal velocity perturbations. Comparisons of experimentally determined and calculated temperature, CO and H_2O mole fraction profiles provide verification of the accuracy of the model.
© 2006 The Combustion Institute. Published by Elsevier Inc. All rights reserved.

Keywords: Diffusion flame; Time-varying; Computation; Diagnostics

1. Introduction

Multidimensional flames have been used to study hydrocarbon flame structure, soot formation and NO_x production. As the level of chemistry increases in complexity in these systems, they are almost always studied under steady, laminar

* Corresponding author. Fax: +1 203 432 6775.
E-mail address: mitchell.smooke@yale.edu (M.D. Smooke).

1540-7489/$ - see front matter © 2006 The Combustion Institute. Published by Elsevier Inc. All rights reserved.
doi:10.1016/j.proci.2006.08.109

flow conditions (see, e.g., [1]). However, practical combustion devices frequently operate under unsteady conditions and the flow field is often turbulent. To be able to model more realistic combustion configurations, time-varying flow fields need to be incorporated into detailed chemistry studies. Depending upon the magnitude of the velocity field variation, time-varying laminar diffusion flames form a class of non-premixed combustion problems that bridge the gap between steady laminar combustion and turbulent combustion. They offer a much wider range of interactions between the chemistry and the flow field than can be examined under steady-state conditions. The complex coupling between chemistry and fluid flow in time-varying laminar flames effectively samples different regimes of temperature, mixture fraction, residence time, strain, and scalar dissipation rates than are observed under steady conditions.

In forced time-varying flames, a periodic fluctuation in time is imposed on the fuel flow rate of a steady laminar flame. The study of these flames helps in understanding the interactions between fluid transport and heat and mass transfer in practical combustion systems. Fundamental studies of these interactions, including detailed combustion chemistry, are critical to an understanding of pollutant formation processes and to the modeling of turbulent diffusion flames through the concept of laminar flamelets. A number of investigators have studied forced, time-varying laminar diffusion flames [2–18]. These investigations have been experimental [2–10], computational [11–13,18] or have combined both experimental and numerical techniques in their approach [14–17].

In this paper, we investigate computationally and experimentally the structure of a forced, time-varying, axisymmetric, coflow, laminar, methane–air diffusion flame. Computationally, we employ a modified vorticity–velocity formulation to solve the transient equations for the conservation of mass, momentum, energy, and chemical species. Experimentally, Rayleigh and Raman scattering are used to obtain two-dimensional fields of temperature, and of mole fractions of N_2, CO_2, CH_4, H_2, O_2, CO, and H_2O. Measurements of excited-state CH (CH^*) emission are used to determine overall flame shape during the initial cycles after the forcing is initiated. Particle image velocimetry (PIV) is used to determine the fuel tube exit velocity and phase over a cycle of the forcing modulation. We compare the different numerical and experimental spatial profiles of temperature and species concentrations at different times in the forcing cycle and we investigate the impact of start-up transients. In the next section, the experimental procedure is described. The problem is then formulated and the computational method is discussed. Results and conclusions are presented in the last two sections.

2. Experimental procedure

2.1. Burner configuration

Atmospheric pressure, axisymmetric, coflowing, nonpremixed laminar flames are generated with a burner in which the fuel flows from an inner tube of radius $R_I = 0.2$ cm (wall thickness 0.038 cm) into a concentric, 3.7 cm radius oxidizer coflow (see Fig. 1). A speaker in the plenum of the fuel jet allows a periodic perturbation to be imposed on the exit parabolic velocity profile. Measurements were made both at Yale and George Washington University. To facilitate measurements at different laboratories on multiple copies of the same burner, it has been designed using computer-aided-design software that is associated with an online machine shop. By submitting the CAD files, which are being made freely available, copies of the burner can be obtained easily.

The fuel contains a mixture of 65% methane and 35% nitrogen, by volume. The addition of nitrogen produces a steady flame with negligible soot. With increasing levels of forcing, the amount of soot in the flame increases [3–8]. An average exit velocity of 35 cm/s is used for both the fuel (parabolic velocity profile) and the oxidizer (plug flow). The flame is lifted approximately 0.6 cm above the burner surface, preventing heat transfer

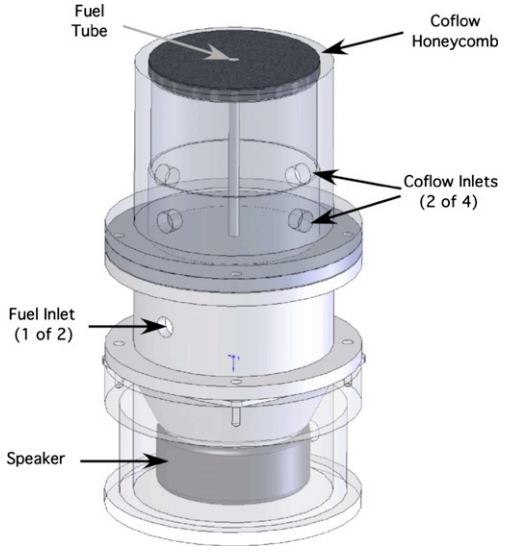

Fig. 1. CAD drawing of the forced-flow burner used in these experiments. Perforated plates in the coflow plenum provide additional flow straightening, but are omitted for clarity.

from the flame to the burner. As a result, room temperature can be used as the boundary condition for the numerical calculations.

2.2. Optical diagnostic measurements

Two-dimensional profiles of temperature and mole fractions of N_2, CO_2, CH_4, H_2, O_2, CO, and H_2O were determined at different phases of the forced flames from vibrational Raman scattering and Rayleigh scattering. Details of the Raman/Rayleigh measurements are similar to those presented by McEnally et al. [19], and will be outlined briefly below. A frequency doubled Nd:YAG laser (532 nm) was focused into a line (300 μm beam waist) over the center of the burner. To prevent breakdown of the gases at the laser focus, the Q-switch was double-pulsed during each flashlamp pulse (100 μs pulse separation, 150 mJ/pulse). The scattered light was imaged onto the entrance of a 0.27 m spectrograph, and the resulting spatial/spectral images were recorded with an image-intensified CCD detector. The spectral coverage of the images allowed the measurement of the Rayleigh scattering as well as the Stokes-shifted vibrational Raman intensities from all major species. Images from 1200 laser pulses were phase-averaged with respect to the burner forcing to improve signal/noise. To account for the effects of broadband fluorescence interference on the Raman signals, data were recorded with polarizations parallel to and perpendicular to the laser polarization. Subtracting the cross polarized images (which contained primarily fluorescence interference) from those with parallel polarization effectively reduced the fluorescence contribution to shot-noise levels. The resulting difference image provided species mole fractions and temperature along a single line in the flame after processing that utilized spectral modeling software and suitable calibration data. Two-dimensional images were formed by tiling together a series of line images. In the images shown, pixel volumes are $0.2 \times 0.3 \times 0.5$ mm^3 near the burner and $0.2 \times 0.3 \times 1$ mm^3 farther downstream, where changes in the axial direction are smaller.

The modulation of the fuel flow for the time-varying flame was calibrated using PIV for each of the burners. The fuel flow was seeded with sugar particles using a TSI six jet atomizer. Two frequency-doubled Nd:YAG lasers (300 μs pulse separation) were focused into a sheet across the burner centerline. PIV images were recorded using a fast interline transfer CCD camera. A cross-correlation algorithm was used to determine the centerline exit velocity as a function of the speaker's forcing level. Forcing levels corresponding to 30% and 50% modulation of the fuel flow were investigated experimentally and computationally. The speaker was driven at 20 Hz.

Chemically excited CH (CH^*) generates flame chemiluminescence through the $A^2\Delta \rightarrow X^2\Pi$ transition at 431.4 nm, and is indicative of the flame front position [20]. This technique was used as a relatively simple experimental means to study the number of cycles required for the steady flame to become fully periodic after the initial forcing was applied. Measurements were taken for 10 cycles immediately following initial forcing. Line-of-sight images were integrated over 100 forcing cycles using an exposure of 1 ms. A 450 nm short-pass filter was used to image CH^*, while a 650 nm long-pass filter provided images used to correct for soot interferences. The axisymmetric images were Abel inverted to obtain the radial profile of relative CH^* concentration [21,22].

3. Problem formulation and numerical solution

The computational model solves the full set of time-dependent, elliptic, partial differential conservation equations for mass, momentum, species and energy [23]. A modified vorticity–velocity formulation [24] is used to compute the velocity field as it does a better job of conserving mass than the formulation in [25]. The system is closed with the ideal gas law and appropriate boundary conditions on each side of the computational domain. The starting estimate for the problem are the corresponding steady diffusion flame solution. To match the experimental setup, the fuel inflow axial velocity boundary condition is set as a parabolic profile that oscillates sinusoidally about an average velocity (both spatially and temporally).

The gas is assumed Newtonian and diffusion is Fickian; the nth species diffusion velocity is calculated using a detailed mixture averaging. The Soret and Dufour effects are neglected; viscous dissipation terms, however, are maintained. The flow's small Mach number implies that the pressure field can be obtained via the ideal gas law. All thermodynamic, chemical, and transport properties are evaluated using vectorized and highly efficient libraries [26]. The divergence of the net radiative flux is calculated using an optically thin radiation submodel with three radiating species (H_2O, CO, and CO_2), the details of which are found in [27,28].

Implementation of a vorticity–velocity formulation for time-dependent problems was anticipated in [25] to cause convergence difficulties for the linear system solver since the Jacobian does not tend toward diagonal dominance for small time steps. Therefore, the traditional approach of shrinking the time step to aid convergence does not work. To maintain desired levels of discretization accuracy without employing extremely small ($<10^{-6}$ s) time steps, second-order temporal discretizations are used. Not only do higher-order

temporal discretizations (and the fully implicit nature of Newton's method) allow the use of larger time steps (between 10^{-6} and 10^{-4} s), but the number of time steps required to cover a time interval of interest is significantly smaller. Also, unlike a primitive variable approach, the purely elliptic nature of the governing equations removes any need for pseudo-time-stepping within each real-time step, resulting in a further speedup. The set of coupled, nonlinear, partial differential equations is discretized using finite differences and solved using a damped, modified Newton's method [29]. At each adaptively chosen timestep [30] the linear Newton equations are solved using Bi-CGSTAB [31] with a block Gauss-Seidel preconditioner. Calculations were performed on a 2.0 GHz AMD Opteron processor with 5 GB RAM.

4. Results and discussion

In this section, we discuss the experimental and computational results for a forced, time-varying, axisymmetric, unconfined, methane–air diffusion flame. While we have utilized a C_2 reaction set in prior work [16], the quantities in which we are interested in this paper can be predicted well with only C_1 chemistry (16 species and 46 reversible reactions [32]). We point out, however, that as one moves towards comparisons of computational and experimental soot volume fractions, the level of chemical complexity (and the CPU time) will increase dramatically. The computational domain covers a region from $r = 0$ to $R_{\max} = 7.5$ cm in the radial direction and $z = 0$ to $z = 40$ cm in the axial direction. The dimensions of the domain are set to values much larger than the radius of the coflowing oxidizer jet, R_O, and the steady flame length, L_f, respectively, so that the asymptotic approach of the solution profile to its free stream value can be predicted accurately.

The time-variation in the flame is produced by imposing a sinusoidal velocity fluctuation on a steady flame, which has a parabolic axial velocity profile with an average velocity of 35 cm/s. Specifically, across the fuel jet, axial velocity $v_z = 70.0(1 - r^2/R_I^2)(1 + \alpha \sin \omega t)$ cm/s, where α is the velocity amplitude factor and ω is the frequency of oscillation. Experiments and computations were performed for velocity perturbations of 30% and 50% of the steady parabolic fuel velocity. Numerical and experimental sinusoidal velocity profiles agree to within 10% of each other over a given cycle. The velocity across the oxidizer jet is 35 cm/s except for a thin boundary layer at the wall. Boundary conditions along the centerline ($r = 0$) are such that radial velocity v_r and radial gradients of all the other unknowns vanish. At the outer boundary $r = R_{\max}$, the radial gradients of v_r and v_z vanish, the temperature is 298 K, and the mass fractions are specified as $Y_{O_2} = 0.232$, $Y_{N_2} = 0.768, Y_k = 0,\ k \neq O_2,\ N_2$. At the outflow boundary, the axial gradients of the unknowns vanish. At the inflow boundary $z = 0$, the radial velocity vanishes and the temperature is 298 K. The mole fractions at the inlet are $Y_{CH_4} = 0.65$, $Y_{N_2} = 0.35$, $Y_k = 0$, $k \neq CH_4$, N_2. Across the fuel tube, and the region where $r > R_O$, v_z vanishes. For $R_I < r < R_{\max}$ at the inlet, the mass fractions are specified as $Y_{O_2} = 0.232$, $Y_{N_2} = 0.768$, $Y_k = 0$, $k \neq O_2$, N_2.

The computations were carried out on a nonuniform computational grid consisting of 137 by 258 adaptively chosen points in the r and z directions, respectively. The points are kept fixed during the computation and were chosen to ensure resolution of the various high activity regions during a velocity cycle. The smallest spacing was 0.005 cm in each direction.

In previous work [16], we were concerned about the length of time necessary for the initial transient features of the problem to die out so that comparisons could be made between the experiments and computations. Specifically, in Fig. 2 (top) we illustrate computational contours of the difference between the computed CH_3 field in the midpoint of a cycle and the computed CH_3 field at the same point in the previous cycle. The experimental contours (bottom) illustrate the same quantities but for CH^*. In both cases, the largest initial transients disappear within several cycles. While the experimental transients are almost totally gone by cycle four, the computational results indicate that some transient effects (while small) are still observable after 10 cycles. The difference in the speed with which these effects die off is partially related to the spatial extent and magnitude of the two species being compared and to the numerical refinement used in the computations. Nevertheless, to explore this issue further, we have defined a correlation function CF(i) as a function of the flame's cycle number i

$$\mathrm{CF}(i) = \frac{\sum_{n=1}^{N\text{points}} \mathrm{Var}_p(i,n) - \mathrm{Var}_p(i-1,n)}{\sum_{n=1}^{N\text{points}} \mathrm{Var}_p(2,n) - \mathrm{Var}_p(1,n)}, \qquad (1)$$

where $\mathrm{Var}_p = CH_3$ mole fraction for the computations and $\mathrm{Var}_p = CH^*$ mole fraction for the experiments. The function is normalized by the sum of the differences in Var_p for the second cycle so that each data set decays from an initial value of 1.0. As illustrated in Fig. 3, the two experimental data sets decay smoothly to values representative of noise, whereas the two numerical data sets decay initially and then fluctuate until cycle 9 for both the 30% and 50% modulations. We anticipate that these oscillations will decrease as the number of cycles increases. However, based upon these results, we will make comparisons using the computational data in cycle 10.

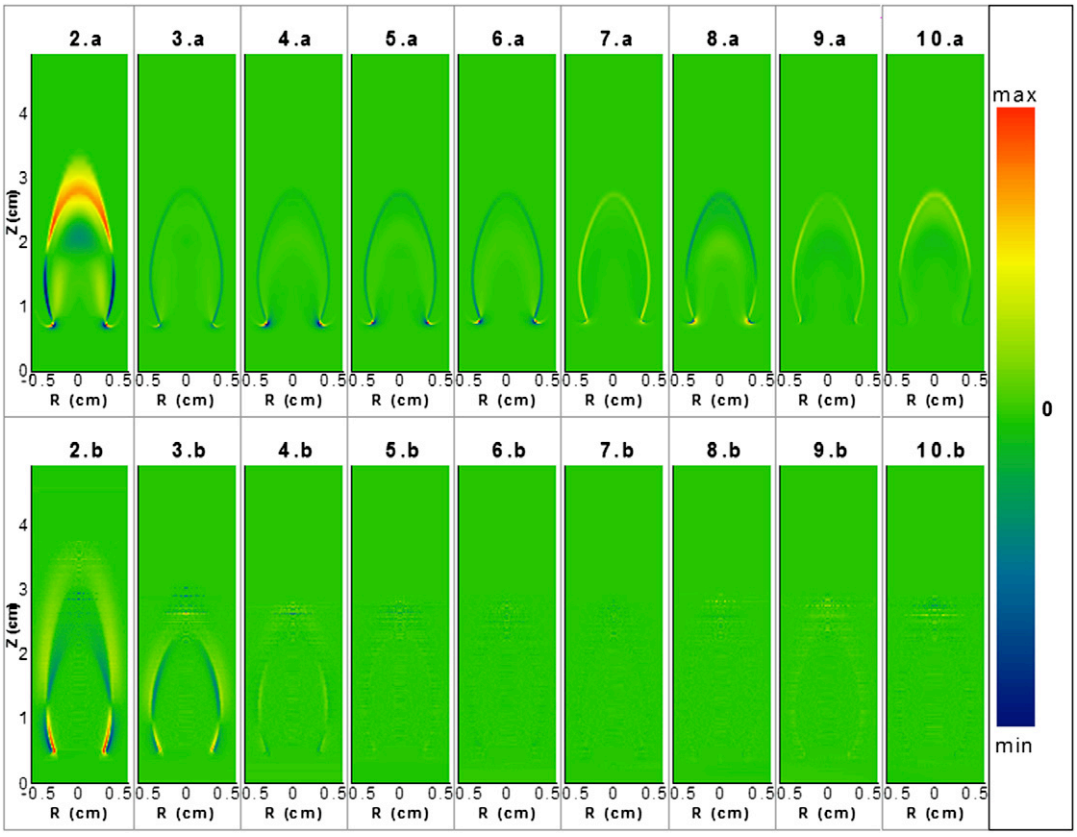

Fig. 2. Computational (top) and experimental (bottom) comparison of the start-up transients in the forced flow burner. Each computational panel illustrates the difference between two consecutive cycles of the CH_3 mole fraction. The experimental panels illustrate the difference between two consecutive cycles of CH^*.

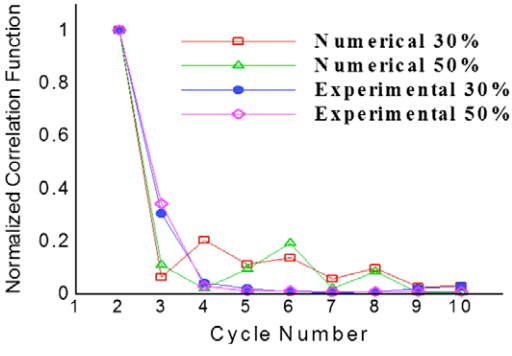

Fig. 3. Correlation function CF(i) versus cycle number.

In Fig. 4, we plot the computed temperature isotherms over a large axial portion of the domain for the steady methane flame along with both the 30% and 50% modulations at the midpoint of a velocity cycle. While the structure of the two flames are similar in the lower two centimetres of the domain, the enhanced modulation produces a more pronounced "pinching" of the temperature profile as one moves higher up in the flame. As we move downstream the effects of the velocity oscillation begin to dampen. Computed and measured isotherms for the 30% modulated flame at 10 ms intervals of the 50 ms cycle are illustrated in Fig. 5. Due to the transient effects observed in Figs. 2 and 3, we have shifted the computational isotherm a few milliseconds compared to the experimental results to line up the features more easily. Frames (b) and (c) have been truncated due to the fact that some soot was formed in the region beyond ~3.5 cm downstream during this part of the oscillation, causing interference with the Raman and Rayleigh measurements.

The flame lift-off height, defined as the smallest z value for which the temperature is greater than 1000 K, was approximately 0.685 cm. In all the frames, the lift-off height remains essentially the same (varying by less than 0.4 mm). However, the flame heights defined by the location of the maximum temperature at the centerline are 4.25 cm in Fig. 5a (7.5 ms), 2.75 cm in Fig. 5b

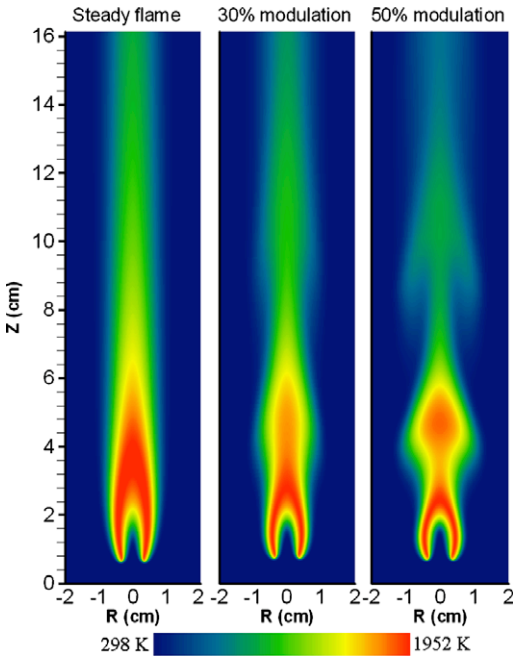

Fig. 4. Computed temperature isotherms for the steady and 30% and 50% modulations in the forced methane–air flame.

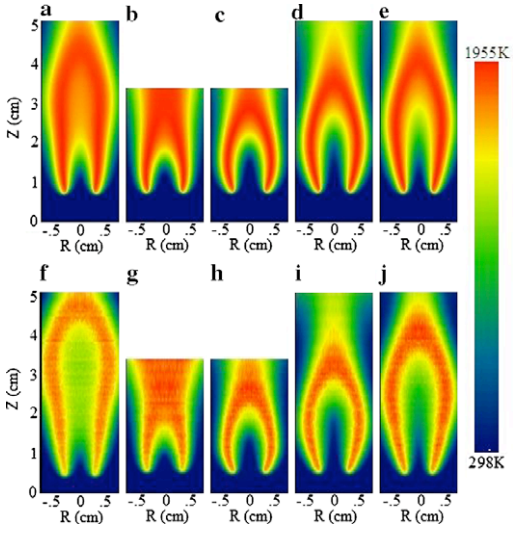

Fig. 5. Computational (a–e) and experimental (f–j) isotherms shown at 10 ms intervals for the 30% modulation flame. Panels b, c, g, and h between 3.5 and 5.0 cm are not shown as these regions exhibit the highest level of particulate interference in Rayleigh imaging.

(17.5 ms), 2.875 cm in Fig. 5c (27.5 ms), 3.5 cm in Fig. 5d (37.5 ms), and 4.0 cm in Fig. 5e (47.5 ms) compared to 3.5 cm for the steady-state case. The maximum temperature during a flame cycle varied between 1963 and 1968 K.

The transient behavior is very different from what we would expect to see in the steady-state case with similar mass flow rates of the fuel. In the steady-state case, the low temperature region above the burner along the axis of symmetry increases and the overall length of the flame gets longer as the fuel mass flow rate is increased. The low temperature core above the burner is smallest for the case of the maximum velocity of the fuel. This behavior can be explained by the fact that, during the time required for the effect of the fluid parcel at the inlet to convect to the flame height, the fuel velocity goes to a minimum. This low temperature region keeps increasing in length even though the velocity keeps decreasing. Overall, the spatial features of the temperature field agree qualitatively between the computations and the experiments.

Profiles for the CO and CO_2 mole fractions are illustrated in Figs. 6 and 7. The panels are at the same time intervals as in Fig. 5. The CO concentration in time-varying laminar flames has been investigated previously [6,10]. In methane flames doped with butane or butene so as to increase their sooting characteristics, it has been reported that increased amounts of soot in a flickering flame result in larger concentrations of CO as well as depletion of OH radicals. Although the 30% flame has minimal soot, we note that there is a 15% increase in the peak CO mole fraction on

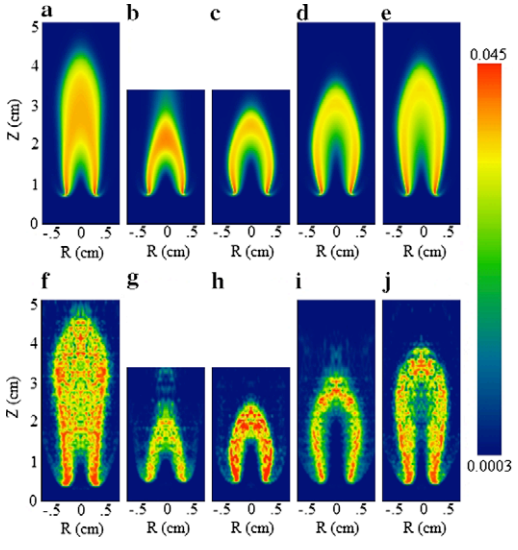

Fig. 6. Computational (a–e) and experimental (f–j) isopleths for CO mole fraction shown at 10 ms intervals for the 30% modulation flame. Panels b, c, g, and h between 3.5 and 5.0 cm are not shown as these regions exhibit the highest level of particulate interference in Rayleigh imaging.

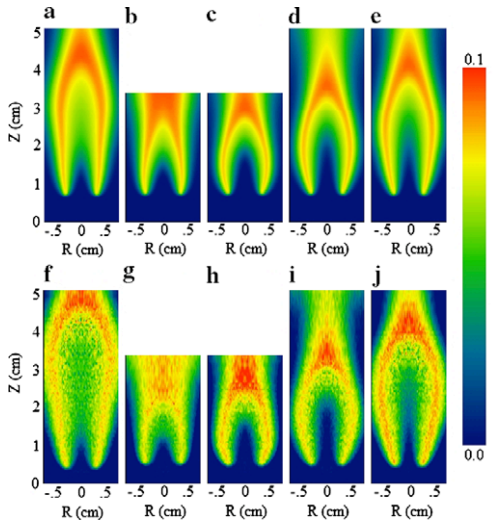

Fig. 7. Computational (a–e) and experimental (f–j) isopleths for CO_2 mole fraction shown at 10 ms intervals for the 30% modulation flame. Panels b, c, g, and h between 3.5 and 5.0 cm are not shown as these regions exhibit the highest level of particulate interference in Rayleigh imaging.

the centerline during the course of a cycle. Whether this increase is due to stretch/strain effects in the chemistry/fluid coupling or soot and polynuclear aromatic hydrocarbon (PAH) oxidation whose products include CO [33] remains uncertain. Future measurements and calculations are planned to study in detail aromatic oxidation chemistry in this flame region.

The oxidation of CO to CO_2 proceeds primarily via the reaction $CO + OH \rightarrow CO_2 + H$. The rate of CO oxidation depends on the availability of OH radicals. However, the presence of most hydrocarbon species inhibits the oxidation of CO. This can be attributed to the fact that the rate of the reaction $H + O_2 \rightarrow OH + O$, is considerably smaller than the reaction rates of H atoms with hydrocarbon species and the rate of the CO oxidation reaction is also smaller than the reaction rates of hydrocarbon species with OH. As a result, small quantities of hydrocarbons can effectively restrict the oxidation of CO to CO_2. Although carbon monoxide and hydrogen are found during the oxidation of the hydrocarbon species, it is not until after the hydrocarbons and the hydrocarbon fragments have been consumed that the OH level rises and CO_2 is formed. This pattern is maintained throughout a flame cycle, i.e., in the axial direction the OH radical pool increases after the disappearance of the methane and the formation of CO. The CO is then oxidized to form CO_2 downstream of the regions of high CH_3, CH_2O, and CO concentrations.

5. Conclusions

We have presented a combined experimental and numerical solution of a forced, time-varying, axisymmetric laminar diffusion flame. Raman and Rayleigh scattering were used to provide a complete series of temperature and major species measurements at 30% and 50% forcing levels for five different phases relative to the forcing. Particle image velocimetry was done to measure the velocity at the exit of the burner and to determine the magnitude and phase of the forcing modulation. Computationally, a fully transient model of methane–air combustion was applied to a flame with a pulsation frequency of 20 Hz. The overall structures of the temperature and major species profiles predicted by the computations were in good qualitative agreement with the experimental measurements. Further investigation is needed into the effects of the magnitude and the frequency of the velocity perturbations on the flame structure.

Acknowledgments

The authors thank the National Science Foundation (Dr. Linda Blevins, contract monitor) for support of this work under Grants CTS-0328296 (Yale) and CTS-0330230 (GWU). In addition, the authors (M.D.S. and M.B.L.) would like to acknowledge support from the DOE Office of Basic Energy Sciences (Dr. Frank Tully, contract monitor) under contract DE-FG02-88ER13966.

References

[1] M.D. Smooke, C.S. McEnally, J. Fielding, et al., *Combust. Theor. Model.* 8 (3) (2004) 593–606.
[2] K.C. Smyth, J.E. Harrington, E.L. Johnson, W.M. Pitts, *Combust. Flame* 95 (1993) 229–239.
[3] C.R. Shaddix, K.C. Smyth, *Combust. Flame* 99 (1994) 723–732.
[4] C.R. Shaddix, K.C. Smyth, *Combust. Flame* 100 (1995) 518.
[5] C.R. Shaddix, K.C. Smyth, *Combust. Flame* 107 (1996) 418–452.
[6] D.A. Everest, C.R. Shaddix, K.C. Smyth, *Proc. Combust. Inst.* 26 (1996) 1161–1169.
[7] K.C. Smyth, C.R. Shaddix, D.A. Everest, *Combust. Flame* 111 (1997) 185–207.
[8] C.R. Shaddix, T.C. Williams, L.G. Blevins, R.W. Schefer, *Proc. Combust. Inst.* 30 (2005) 1501–1508.
[9] O.A. Ezekoye, K.M. Martin, F. Bisetti, *Proc. Combust. Inst.* 30 (2005) 1485–1492.
[10] R.R. Skaggs, J.H. Miller, *Proc. Combust. Inst.* 26 (1996) 1181–1188.
[11] S. Mahalingam, B.J. Cantwell, J.H. Ferziger, *Phys. Fluids A* 2 (1990) 720–728.
[12] F.N. Egolfopoulos, C.S. Campbell, *J. Fluid Mech.* 318 (1996) 1–29.
[13] R.B. Pember, L.H. Howell, J.B. Bell, P. Collela, W.Y. Crutchfield, W.A. Fiveland, et al. *Western*

States Section of the Combustion Institute, Livermore, CA, 1997.
[14] C.R. Kaplan, C.R. Shaddix, K.C. Smyth, *Combust. Flame* 106 (1996) 392–405.
[15] H.N. Najm, R.W. Schefer, R.B. Milne, C.J. Mueller, K.D. Devine, S.N. Kempka, SAND98-8232, Sandia National Laboratories Report, 1998.
[16] R.K. Mohammed, M.A. Tanoff, M.D. Smooke, A.M. Schaffer, M.B. Long, *Proc. Combust. Inst.* 27 (1998) 693–702.
[17] P.H. Renard, D. Thevenin, J.C. Rolon, S. Candel, *Prog. In Energy and Comb. Sci.* 26 (2002) 225–282.
[18] M.S. Day, J.B. Bell, *Combust. Theor. Model.* 4 (2000) 221–258.
[19] C.S. McEnally, L.D. Pfefferle, A.M. Schaffer, et al., *Proc. Combust. Inst.* 28 (2000) 2063–2070.
[20] J. Luque, J.B. Jeffries, G.P. Smith, et al., *Combust. Flame* 122 (1–2) (2000) 172–175.
[21] C.J. Dasch, *Appl. Opt.* 31 (1992) 1146–1152.
[22] K.T. Walsh, J. Fielding, M.B. Long, *Opt. Lett.* 25 (2000) 457.
[23] B.A.V. Bennett, J. Fielding, R.J. Mauro, M.B. Long, M.D. Smooke, *Combust. Theor. Model.* 3 (1999) 657–687.
[24] S.B. Dworkin, B.A.V. Bennett, M.D. Smooke, *J. Comput. Phys.* 215 (2006) 430–447.
[25] A. Ern, 1994. *Vorticity–velocity modeling of chemically reacting flows*. Ph.D. thesis, Yale University, Mechanical Engineering Department.
[26] V. Giovangigli, N. Darabiha, in: C.M. Brauner, C. Schmidt-Laine (Eds.), *Vector Computers and Complex Chemistry Combustion, in Mathematical Modeling in Combustion and Related Topics*, Nijhoff, Dordrecht, 1988, pp. 491–503.
[27] R.J. Hall, *J. Quantum Spectrosc. Radiat. Transfer.* 49 (1993) 517–523.
[28] R.J. Hall, *J. Quantum Spectrosc. Radiat. Transfer* 51 (1994) 635–644.
[29] M.D. Smooke, *J. Opt. Theory Appl.* 39 (1983) 489–511.
[30] M.D. Smooke, R.E. Mitchell, D.E. Keyes, *Combust. Sci. Tech.* 67 (1989) 85–122.
[31] H.A. Van Der Vorst, *SIAM J. Statist. Comput.* 13 (1992) 631–644.
[32] M.D. Smooke, I.K. Puri, K. Seshadri, *Proc. Combust. Inst.* 21 (1986) 813–821.
[33] R.R. Skaggs, J.H. Miller, *Combust. Flame* 100 (1995) 430–439.